Editors' Suggestion

Higgs Mode of Planar Coupled Spin Ladders and its Observation in $C_9H_{18}N_2CuBr_4$

T. Ying,[1,2] K. P. Schmidt,[3] and S. Wessel[1]
[1]Institut für Theoretische Festkörperphysik, JARA-FIT and JARA-HPC, RWTH Aachen University, 52056 Aachen, Germany
[2]Department of Physics, Harbin Institute of Technology, 150001 Harbin, China
[3]Institut für Theoretische Physik, FAU Erlangen-Nürnberg, 91058 Erlangen, Germany

(Received 22 December 2018; published 25 March 2019)

Polarized inelastic neutron scattering experiments recently identified the amplitude (Higgs) mode in $C_9H_{18}N_2CuBr_4$, a two-dimensional near-quantum-critical spin-1/2 two-leg ladder compound, which exhibits a weak easy-axis exchange anisotropy. Here, we theoretically examine the dynamic spin structure factor of such planar coupled spin-ladder systems using large-scale quantum Monte Carlo simulations. This allows us to provide a quantitative account of the experimental neutron scattering data within a consistent quantum spin model. Moreover, we trace the details of the continuous evolution of the amplitude mode from a two-particle bound state of coupled ladders in the classical Ising limit all the way to the quantum spin-1/2 Heisenberg limit with fully restored SU(2) symmetry, where it gets overdamped by the two-magnon continuum in neutron scattering.

DOI: 10.1103/PhysRevLett.122.127201

A central aspect of current research in quantum magnetism is the exploration of emerging phases and quantum phase transition and the associated collective excitations of quantum matter. For one of the most fundamental ordering phenomena in quantum magnetism—antiferromagnetism from spontaneous SU(2) spin symmetry breaking—the collective excitations can be characterized as fluctuations in the phase and the amplitude of the order parameter field. The phase oscillations correspond to low-energy magnon modes, i.e., gapless Nambu-Goldstone bosons, which are readily detected in inelastic neutron scattering (INS) experiments. However, in low-dimensional systems, for which quantum fluctuations prevail, the Higgs mode, associated to the amplitude fluctuations, is prone to decay into pairs of Nambu-Goldstone modes [1–3]. In low-dimensional magnets, the Higgs mode thus gets strongly masked by this coupling to the two-magnon continuum, which makes its detection formidable by magnetic probes such as INS [4,5]. However, near-quantum-critical systems were recently found to be advantageous for the detection of the Higgs mode in 2D systems via its response in scalar susceptibilities as opposed to the magnetic response accessed in, e.g., INS experiments [1,2,6–10].

A feasible route towards the observation of the Higgs mode in near-quantum-critical low-dimensional magnets was explored in a recent INS study [11] of the layered system of coupled spin ladders in the metal-organic compound $C_9H_{18}N_2CuBr_4$, abbreviated as DLCB. In this compound, the spin-1/2 degrees of freedom on the Cu^{2+} ions experience a weakly anisotropic, easy-axis spin-exchange interaction [12]. This anisotropy gaps out the two-magnon scattering continuum sufficiently above the spectral support of the lower-lying Higgs mode, which acquires an infinite lifetime. The Higgs mode can thus be identified by spin-polarized INS through the longitudinal, (non-spin-flip) channel, where the neutrons' polarization is vertical to the scattering plane, separated from the magnon branch in the transverse (spin-flip) channel [11]. A 2D array of coupled spin ladders furthermore exhibits a line of quantum critical points in a parameter regime that separates the antiferromagnetic ground state from the quantum disordered regime at weak interladder coupling [13]. Being located near such a quantum critical point, a quantitative theory of the quantum spin dynamics in DLCB requires an approach that accounts for both the enhanced quantum critical fluctuations as well as the subtle energetics of the weakly anisotropic exchange.

Here, we demonstrate such a quantitative theoretical characterization of the quantum spin dynamics in coupled spin ladders with anisotropic exchange: Given the absence of geometric frustration in the exchange geometry derived for DLCB [11,12], an unbiased approach for calculating the dynamic spin structure factor (DSF) is shown to be feasible using state-of-the-art quantum Monte Carlo (QMC) methods. In addition to modeling the INS experiments on DLCB, we harness the QMC approach in order to systematically examine the evolution of the magnetic excitations from the isotropic (Heisenberg) limit with its full SU(2) symmetry, down to the Ising-model limit for dominant easy-axis exchange. The Higgs mode, which becomes overdamped in the Heisenberg limit, then connects to a gapped two-magnon bound state in the Ising-model regime. In contrast, for weakly coupled ladders, the same mode instead condenses, and gives rise to a quantum disordered phase.

In the following, we consider as a minimal model [12] for DLCB the quantum spin-1/2 Hamiltonian of a 2D array of coupled two-leg spin-ladders,

$$H = J_{\mathrm{rung}} \sum_{i,r} \lambda (S^x_{i,r,1} S^x_{i,r,2} + S^y_{i,r,1} S^y_{i,r,2}) + S^z_{i,r,1} S^z_{i,r,2} + J_{\mathrm{leg}} \sum_{i,r,l} \lambda (S^x_{i,r,l} S^x_{i,r+1,l} + S^y_{i,r,l} S^y_{i,r+1,l}) + S^z_{i,r,l} S^z_{i,r+1,l} + J_{\mathrm{inter}} \sum_{i,r} \lambda (S^x_{i,r,2} S^x_{i+1,r,1} + S^y_{i,r,2} S^y_{i+1,r,1}) + S^z_{i,r,2} S^z_{i+1,r,1}, \quad (1)$$

where i indexes the ladders, r the rungs, and $l = 1, 2$ the two legs of each ladder. J_{inter} denotes the nearest-neighbor interladder coupling, and J_{leg} (J_{rung}) the intraladder couplings along the legs (rungs), respectively (cf. the inset of Fig. 1). Furthermore, λ is the exchange anisotropy, with $0 \leq \lambda < 1$ in the easy-axis regime, which is considered equal among all exchange interactions [12]. The Heisenberg limit is recovered at $\lambda = 1$, while for $\lambda = 0$, H reduces to a classical Ising model. An explicit constraint on the parameters in Eq. (1) for DLCB follows from its magnetic saturation field of $H_{\mathrm{sat}} \approx 16$ T, i.e.,

$$\frac{1+\lambda}{2}(J_{\mathrm{rung}} + 2J_{\mathrm{leg}} + J_{\mathrm{inter}}) = g\mu_B H_{\mathrm{sat}} \approx 1.96 \text{ meV}, \quad (2)$$

based on a value of $g = 2.12$ [14]. From comparing the low-temperature INS spectra to magnon dispersions obtained within a perturbative continuous unitary transformation (PCUT) approach, Ref. [12] reports the best-fit values $J_{\mathrm{rung}} = 0.64(9)$ meV, $J_{\mathrm{leg}} = 0.60(2)$ meV, $J_{\mathrm{inter}} = 0.19(2)$ meV, and $\lambda = 0.93(2)$. These parameters position DLCB close to quantum criticality, where the long-range antiferromagnetic order along the easy-axis direction vanishes: In the Heisenberg limit ($\lambda = 1$) for spatially isotropic ladders ($J_{\mathrm{rung}} = J_{\mathrm{leg}}$), this quantum critical point is located at a critical ratio of $J_{\mathrm{inter}}/J_{\mathrm{leg}} = 0.314\,07(5)$ [13]. The value of $\lambda < 1$ is in accord with the constraint in Eq. (2), and accounts for the finite excitation gaps $\Delta_{\mathrm{TM}} = 0.33(3)$ meV and $\Delta_{\mathrm{LM}} = 0.48(3)$ meV, estimated in polarized INS for the transverse magnon mode (TM) and the longitudinal Higgs mode (LM), respectively [11]. A finite Δ_{TM} not only renders the Nambu-Goldstone mode from the isotropic case massive, it also leads to a minimum excitation energy of $2\Delta_{\mathrm{TM}}$ for the two-magnon continuum. For $\Delta_{\mathrm{LM}} < 2\Delta_{\mathrm{TM}}$, the Higgs mode is protected against decay into the two-magnon continuum, thus allowing for its identification in the longitudinal scattering channel [11]. The theoretical modeling of the INS data in this configuration was performed in Ref. [11] using bond-operator theory in harmonic approximation [15,16]. However, within this mean-field treatment, the comparison to the experimental data required a substantial renormalization of the exchange couplings in the Hamiltonian of Eq. (1), up to factors of almost 2, compared to the values quoted above. This calls for an unbiased, consistent theoretical understanding of the INS results on DLCB, which applies to *both* scattering channels, and also accounts for the critically enhanced quantum fluctuations.

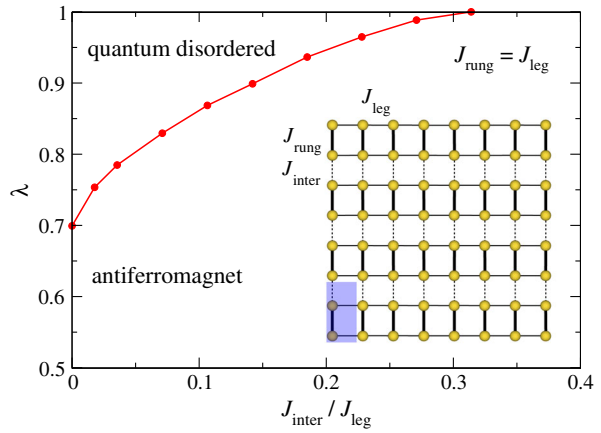

FIG. 1. Ground-state phase diagram of a 2D array of coupled spin-1/2 ladders with easy-axis anisotropy λ and $J_{\mathrm{rung}} = J_{\mathrm{leg}}$. Inset: 2D array of coupled ladders ($L = 4$ ladders, $L_r = 8$ rungs per ladder), with a two-site unit cell as indicated.

For this purpose, we analyzed the DSF of the Hamiltonian H using a combination of QMC simulations [17–20] and a stochastic analytical continuation scheme [21] in order to access the frequency-dependent spectral functions from imaginary-time correlation functions obtained by the QMC calculations. We thereby obtain the DSF for both the longitudinal channel, $S_L(\boldsymbol{k}, \omega) = \int dt e^{-i\omega t} \langle S^z_{\boldsymbol{k}}(t) S^z_{-\boldsymbol{k}}(0) \rangle$, as well as for the transverse channel, $S_T(\boldsymbol{k}, \omega) = \int dt e^{-i\omega t} \langle S^+_{\boldsymbol{k}}(t) S^-_{-\boldsymbol{k}}(0) + S^-_{\boldsymbol{k},}(t) S^+_{-\boldsymbol{k}}(0) \rangle$ [22]. Here, $\boldsymbol{S}_{\boldsymbol{k}} = (1/\sqrt{N}) \sum_i e^{-i\boldsymbol{k}\cdot\boldsymbol{r}_i} \boldsymbol{S}_i$, and N denotes the number of spins, with $N = 2LL_r$ in terms of the number of ladders (L) and rungs per ladder (L_r), with periodic boundary conditions taken in both lattice directions (the unit cell contains two spins, cf. the inset of Fig. 1, and the extent of the unit cell is set equal to unity in both lattice directions). For the QMC simulations, performed using the stochastic series expansion approach [17–19], we scaled $L_r = 2L$ and the temperature T sufficiently low to access ground-state properties of these finite systems [22].

Prior to focusing on DLCB, we consider the simpler case of spatially isotropic ladders ($J_{\mathrm{rung}} = J_{\mathrm{leg}}$), for which the ground-state phase diagram in terms of the ratio $J_{\mathrm{inter}}/J_{\mathrm{leg}}$ and λ, as obtained from QMC simulations, is shown in Fig. 1. In addition to a phase with antiferromagnetic order, this phase diagram exhibits an extended quantum disordered regime at weak interladder coupling near the Heisenberg limit. For $\lambda < 1$, a line of quantum critical points separates both phases, belonging to the three-dimensional (3D) Ising universality class, in accord with a standard finite-size scaling analysis of the antiferromagnetic structure factor [22]. For $\lambda = 1$, the quantum critical point at $J_{\mathrm{inter}}/J_{\mathrm{leg}} = 0.314\,07(5)$ instead belongs to the 3D Heisenberg universality class [13].

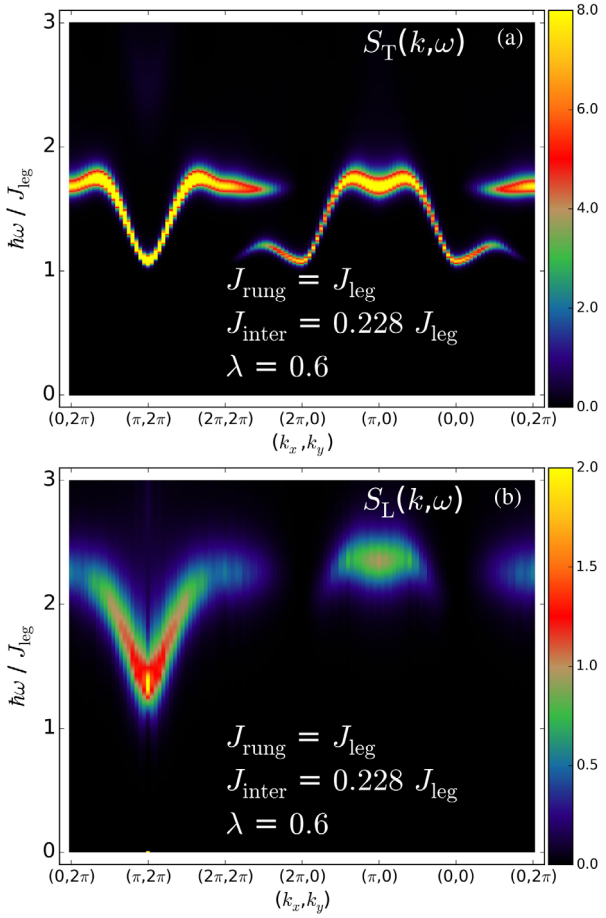

FIG. 2. DSF of a 2D array of coupled spin ladders, (a) $S_T(\boldsymbol{k},\omega)$ and (b) $S_L(\boldsymbol{k},\omega)$, for $J_{\text{rung}} = J_{\text{leg}}$, $J_{\text{inter}} = 0.228 J_{\text{leg}}$, and $\lambda = 0.6$, along the indicated path in momentum space, obtained by QMC simulations with $L = 20$ at $T = 0.02 J_{\text{leg}}$.

We now examine in detail the evolution of the DSF upon tuning λ for $J_{\text{inter}}/J_{\text{leg}} = 0.228$ and 0.4, i.e., on both sides of the critical coupling ratio for $\lambda = 1$. These two different regimes are denoted as case I and II, respectively. As an example, Fig. 2 displays the DSF for $J_{\text{inter}}/J_{\text{leg}} = 0.228$ and $\lambda = 0.6$, along the indicated path in momentum space that includes the antiferromagnetic ordering vector $\boldsymbol{k}_{\text{AFM}} = (\pi, 2\pi)$. The transverse channel $S_T(\mathbf{k},\omega)$ is dominated by the gapped magnon excitation, with a minimum gap $\Delta_{\text{TM}} \approx 1.1 J_{\text{leg}}$ at $\boldsymbol{k}_{\text{AFM}}$. This sets the lower threshold for the two-magnon continuum to $2\Delta_{\text{TM}} \approx 2.2 J_{\text{leg}}$. Besides the magnetic Bragg peak at $\boldsymbol{k}_{\text{AFM}}$, $S_L(\mathbf{k},\omega)$ exhibits an additional, pronounced dispersing mode at energies significantly below $2\Delta_{\text{TM}}$, and with a corresponding minimum gap of $\Delta_{\text{LM}} \approx 1.3 J_{\text{leg}}$ at $\boldsymbol{k}_{\text{AFM}}$. Its origin becomes explicit in the Ising limit: For $\lambda = 0$, the ground states are perfect Néel configurations, and a single spin flip costs an excitation energy $\Delta_{\text{TM}} = (J_{\text{rung}} + 2J_{\text{leg}} + J_{\text{inter}})/2$. A bound state of two nearest-neighbor spin flips along an intraladder bond (for $J_{\text{rung}} = J_{\text{leg}} > J_{\text{inter}}$) requires an energy $\Delta_{\text{LM}} = 2J_{\text{leg}} + J_{\text{inter}}$, which falls below the excitation energy $2\Delta_{\text{TM}}$

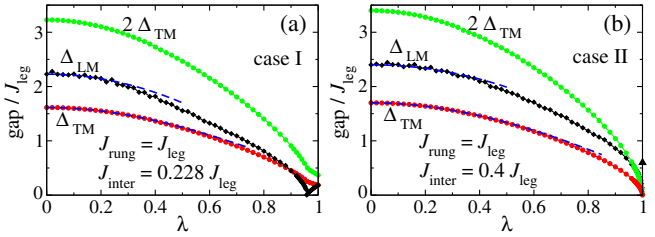

FIG. 3. Excitation gaps Δ_{TM}, $2\Delta_{\text{TM}}$, and Δ_{LM} as functions of λ at $J_{\text{rung}} = J_{\text{leg}}$ for (a) $J_{\text{inter}} = 0.228 J_{\text{leg}}$ (case I) and (b) $J_{\text{inter}} = 0.4 J_{\text{leg}}$ (case II). Dashed lines show results from series expansions. The triangle in (b) shows the position of the Higgs mode for $\lambda = 1$ from the dynamic singlet structure factor.

for two isolated spin flips. The transverse exchange for finite values of λ renders these modes dispersive, thereby reducing both excitation gaps.

From QMC data such as in Fig. 2, we extract the full λ dependence of both gaps in the thermodynamic limit [22], cf. Fig. 3. Also shown in this figure are series expansion results [11,22,24] up to order λ^2 (λ^8) for Δ_{LM} (Δ_{TM}), which closely follow the QMC data up to intermediate values of λ. For case I, at $J_{\text{inter}}/J_{\text{leg}} = 0.228$ [Fig. 3(a)], we identify the quantum critical point at $\lambda_c = 0.964(2)$, where Δ_{LM} closes. Δ_{TM} stays finite across the transition, exhibiting an inflection point. While in the antiferromagnetic regime, $\lambda < \lambda_c$, the LM mode connects to a two-spin-flip bound state of the Ising limit, it forms the $S^z = 0$ sector of the gapped triplon mode in the quantum disordered regime, which is degenerate with the TM mode of the transverse branch in the Heisenberg limit. The LM mode resides below the two-magnon continuum of energies above $2\Delta_{\text{TM}}$ for all λ. For case II, at $J_{\text{inter}}/J_{\text{leg}} = 0.4$ [Fig. 3(b)], the antiferromagnetic regime extends up to the Heisenberg limit, in which the TM gap closes. The softening of Δ_{TM} affects the LM mode to merge into the two-magnon continuum, which we locate to occur at $\lambda_m = 0.96(2)$. Beyond this point, the detection of the Higgs mode is masked by the two-magnon continuum. Close to quantum criticality and in the Heisenberg limit ($\lambda = 1$), one may nevertheless detect the Higgs mode through the scalar susceptibility in terms of the rung-based dynamic singlet structure factor [10,25,26]. The position of the Higgs mode from this scalar response function is also shown in Fig. 3(b); it compares well to the energy of the LM mode near λ_m.

We next return to the theoretical modeling of the INS spectra for DLCB. Since this compound resides within the antiferromagnetically ordered regime of coupled spin ladders, we first assess to which of the two cases (I or II) it belongs, according to the effective description by the model in Eq. (1). For this purpose, we performed QMC simulations for the set of previously estimated exchange couplings, but vary the anisotropy λ. We observe from Fig. 4 that based on this parameter set, DLCB actually belongs to case I; i.e., for the estimated exchange

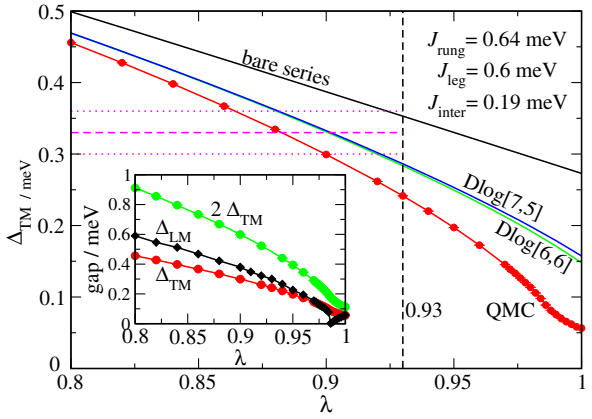

FIG. 4. Excitation gap Δ_{TM} from QMC and PCUTs (bare order λ^8 series and Dlog-Padé approximants) as functions of λ for $J_{leg} = 0.6$ meV, $J_{rung} = 0.64$ meV, and $J_{inter} = 0.19$ meV. Horizontal lines set the margin of the INS estimate $\Delta_{TM} = 0.33(3)$ meV for DLCB from Ref. [11]. The inset shows Δ_{TM}, Δ_{LM}, and $2\Delta_{TM}$ as functions of λ as obtained from QMC simulations.

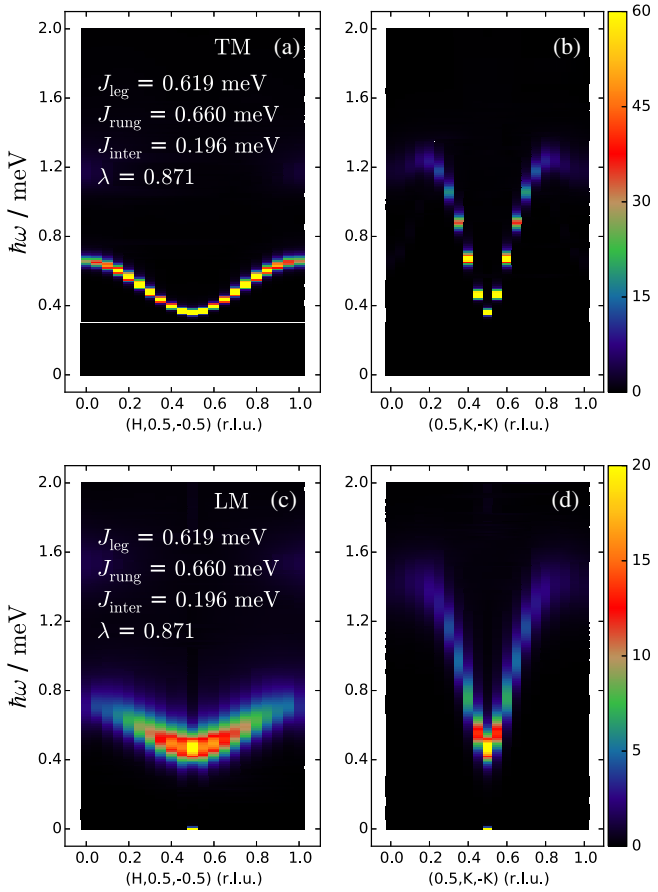

FIG. 5. Scattering spectra for DLCB as a function of energy and wave vector transfer in the transverse (a),(b) and longitudinal (c),(d) configurations, exhibiting the TM and LM modes, respectively. Data based on QMC simulations ($L = 20$) of the 2D model H for the displayed parameters.

couplings, H resides within the quantum disordered regime at $\lambda = 1$: The easy-axis anisotropy not only leads to finite magnetic excitation gaps, it also leads out of the quantum disordered regime. The presence of a quantum phase transition at $\lambda_c = 0.989(1)$ (detected also by the antiferromagnetic structure factor [22]) for this set of couplings was not noted in Refs. [11,12], wherein PCUT-based estimates of Δ_{TM} were used instead. As shown in Fig. 4, this approach does not reproduce the inflection point in Δ_{TM} at λ_c and overestimates the gap in the relevant parameter regime. Therefore, the gap $\Delta_{TM} \approx 0.24$ meV extracted from the QMC calculations at the previously estimated value of $\lambda = 0.93$ falls below the experimental margin for DLCB; i.e., a lower value of λ is required to match the experimental values of the gaps for the considered exchange coupling strengths. Agreement with the experimental estimates of the gaps within their error margins can be reached using a simple rescaling procedure: In order to satisfy Eq. (2), a decrease in λ requires a corresponding increase of the exchange coupling strengths. Here, we constrain to a uniform rescaling of all exchange constants for simplicity. Using an interpolation of the QMC data in Fig. 4 [22], we obtain $J_{leg} = 0.619$ meV, $J_{rung} = 0.660$ meV, $J_{inter} = 0.196$ meV, and $\lambda = 0.871$, for which $\Delta_{TM} = 0.360$ meV and $\Delta_{LM} = 0.457$ meV; i.e., both values are within the margin of the experimental estimates. We thus spared a fit of all four parameters of H to the INS data, which is rather expensive based on QMC calculations of the DSF.

Based on this consistent identification of a single set of model parameters for DLCB, we finally performed QMC simulations to calculate the corresponding DSF. To allow for a direct comparison to the INS results presented in Ref. [11], we transformed the QMC spectra [22] to the crystal and scattering geometry for DLCB [11]. The resulting scattering spectra along the specific wave vector transfers considered in Ref. [11] are shown in Fig. 5 for both polarization directions. They correspond to the polarized INS data shown in Fig. 4 of Ref. [11]. In addition to the excitation gaps and the overall distribution of the spectral weight, the calculated spectra also account for the bandwidth observed in the INS spectra in the LM scattering channel at the zone boundary, which was overestimated in the harmonic bond-operator theory approach from Ref. [11].

Hence, we demonstrated the feasibility, using state-of-the-art QMC simulation techniques, to formulate a quantitative theory for the spin dynamics of near-quantum-critical 2D quantum magnets, directly exposing the two-magnon bound-state nature of the stable Higgs mode excitation observed in recent INS experiments on DLCB. In the easy-axis regime, this excitation is stabilized due to the upwards-shifted support of the two-magnon continuum, well above the Higgs mode's excitation gap. The Higgs mode merges into this continuum only very close to the Heisenberg limit

within the antiferromagnetic regime, beyond the quantum critical point. We anticipate that our unbiased QMC approach provides a quantitative understanding to the quantum spin dynamics also in other near-quantum-critical 2D magnetic compounds.

We thank Tao Hong for valuable discussions. This work was supported by the Deutsche Forschungsgemeinschaft (DFG) under Grants No. FOR 1807 and No. RTG 1995, as well as the National Natural Science Foundation of China under Grant No. 11504067. We thank the IT Center at RWTH Aachen University and the Jülich Supercomputing Centre for access to computing time through JARA-HPC.

[1] D. Podolsky, A. Auerbach, and D. P. Arovas, Phys. Rev. B **84**, 174522 (2011).
[2] D. Podolsky and S. Sachdev, Phys. Rev. B **86**, 054508 (2012).
[3] D. Pekker and C. M. Varma, Annu. Rev. Condens. Matter Phys. **6**, 269 (2015).
[4] I. Affleck and G. F. Wellman, Phys. Rev. B **46**, 8934 (1992).
[5] S. A. Weidinger and W. Zwerger, Eur. Phys. J. B **88**, 237 (2015).
[6] L. Pollet and N. V. Prokof'ev, Phys. Rev. Lett. **109**, 010401 (2012).
[7] K. Chen, L. Liu, Y. Deng, L. Pollet, and N. V. Prokof'ev, Phys. Rev. Lett. **110**, 170403 (2013).
[8] S. Gazit, D. Podolsky, and A. Auerbach, Phys. Rev. Lett. **113**, 240601 (2014).
[9] A. Rançon and N. Dupuis, Phys. Rev. B **89**, 180501(R) (2014).
[10] M. Lohöfer and S. Wessel, Phys. Rev. Lett. **118**, 147206 (2017).
[11] T. Hong, M. Matsumoto, Y. Qiu, W. Chen, T. R. Gentile, S. Watson, F. F. Awwadi, M. M. Turnbull, S. E. Dissanayake, H. Agrawal, R. Toft-Petersen, B. Klemke, K. Coester, K. P. Schmidt, and D. A. Tennant, Nat. Phys. **13**, 638 (2017).
[12] T. Hong, K. P. Schmidt, K. Coester, F. F. Awwadi, M. M. Turnbull, Y. Qiu, J. A. Rodriguez-Rivera, M. Zhu, X. Ke, C. P. Aoyama, Y. Takano, H. Cao, W. Tian, J. Ma, R. Custelcean, H. D. Zhou, and M. Matsuda, Phys. Rev. B **89**, 174432 (2014).
[13] M. Matsumoto, C. Yasuda, S. Todo, and H. Takayama, Phys. Rev. B **65**, 014407 (2001).
[14] T. Hong, Y. Qiu, M. Matsumoto, D. A. Tennant, K. Coester, K. P. Schmidt, F. F. Awwadi, M. M. Turnbull, H. Agrawal, and A. L. Chernyshev, Nat. Commun. **8**, 15148 (2017).
[15] S. Sachdev and R. N. Bhatt, Phys. Rev. B **41**, 9323 (1990).
[16] T. Sommer, M. Vojta, and K. W. Becker, Eur. Phys. J. B **23**, 329 (2001).
[17] A. W. Sandvik, Phys. Rev. B **59**, R14157 (1999).
[18] O. F. Syljuasen and A. W. Sandvik, Phys. Rev. E **66**, 046701 (2002).
[19] F. Alet, S. Wessel, and M. Troyer, Phys. Rev. E **71**, 036706 (2005).
[20] F. Michel and H. G. Evertz, arXiv:0705.0799; F. Michael, Ph. D. thesis, University of Graz, 2007.
[21] K. S. D. Beach, arXiv:cond-mat/0403055.
[22] See Supplemental Material at http://link.aps.org/supplemental/10.1103/PhysRevLett.122.127201 for further details on (i) the DSF calculations, (ii) the finite-size scaling analysis, (iii) the determination of the excitation gaps, (iv) the series expansion calculations, (v) the estimation of the parameters for DLCB, and (vi) the transformation of the DSF to the geometry for DLCB, which contains Refs. [11,12,14,20,23,25].
[23] S. El-Showk, M. F. Paulos, D. Poland, S. Rychkov, D. Simmons-Duffin, and A. Vichi, J. Stat. Phys. **157**, 869 (2014).
[24] S. Dusuel, M. Kamfor, K. P. Schmidt, R. Thomale, and J. Vidal, Phys. Rev. B **81**, 064412 (2010).
[25] M. Lohöfer, T. Coletta, D. G. Joshi, F. F. Assaad, M. Vojta, S. Wessel, and F. Mila, Phys. Rev. B **92**, 245137 (2015).
[26] Y. Q. Qin, B. Normand, A. W. Sandvik, and Z. Y. Meng, Phys. Rev. Lett. **118**, 147207 (2017).